Hindawi
Advances in Civil Engineering
Volume 2024, Article ID 5599356, 16 pages
https://doi.org/10.1155/2024/5599356

Research Article

Estimating the Climate-Controlled Soil Parameters and the Distorted Mound Shape for Analysis of Stiffened Rafts on Expansive Soils

Mohamed H. Abu-Ali,[1] **Basuony El-Garhy**,[1] **Ahmed Boraey**,[1] **Wael S. Al-Rashed**,[1] **and Hassan Abdel-Daiem**[2]

[1]*Department of Civil Engineering, University of Tabuk, P.O. Box 741, Tabuk 71491, Saudi Arabia*
[2]*Department of Electrical Engineering, University of Tabuk, P.O. Box 741, Tabuk 71491, Saudi Arabia*

Correspondence should be addressed to Mohamed H. Abu-Ali; mabuali@ut.edu.sa

Received 7 August 2023; Revised 22 January 2024; Accepted 23 January 2024; Published 7 February 2024

Academic Editor: Paolo Castaldo

A stiffened raft is considered one of the efficient foundation systems for lightweight structures resting on expansive soils. Most existing design methods of stiffened rafts require an analysis of the interaction between the raft and the distorted mound shape of the expansive soil. In most design methods, the distorted mound shape is represented in 2D by the edge distance and the maximum differential movement through a nonlinear equation. This study presents a rational method for estimating the climate-controlled soil parameters that are used for estimating the 3D distorted mound shape of the expansive soil from the routine geotechnical tests' results. These parameters include the equilibrium soil suction, the amplitude of surface suction change, the diffusion coefficient of the soil, the suction compression index, and the active zone depth. The proposed method is explained through its application to calculate the climate-controlled parameters for expansive soils in different locations throughout Saudi Arabia. A parametric study is carried out using a suction diffusion and soil movements program called SUCH to investigate the effect of the climate-controlled soil parameters and raft dimensions on the shape of the distorted mound, maximum differential movement, and edge moisture variation distance. The results of the parametric study are used in a regression analysis to develop an equation for estimating the edge moisture variation distance, which is considered a major barrier to using existing design methods of stiffened rafts as a function of the climate-controlled soil parameters and the aspect ratio of the raft. The findings indicate that the aspect ratio of the raft and the climate-controlled soil parameters have a significant effect on the shape of the distorted mound, its maximum differential movement, and its edge moisture variation distance. Additionally, the proposed equation of the edge moisture variation distance predicts comparable values to that estimated by the program SUCH.

1. Introduction

Expansive soil is one of the problematic soils that exist in the Kingdom of Saudia Arabia, KSA, and in different countries in the Middle East and the world. Expansive soils cause damages, ranging from minor to severe cracks, in the lightweight structures after being constructed. The causes of such cracks include the movements in the supporting expansive soils, the inappropriate identification and classification of expansive soils, as well as the inappropriate selection and design of the foundation systems. Millions of dollars have been lost due to the damage to structures in countries around the world in which expansive soils have existed, including the KSA [1–4]. Therefore, Jones and Holtz [1] described the expansive soil in the United States as "the hidden disaster."

Lightweight structures constructed on expansive soils are frequently subjected to severe movements (shrinkage or heave) arising from nonuniform soil moisture changes, with consequent cracking and damage related to the distortion. Damages of lightweight structures caused by the movements of expansive soil have been reported in many literature (e.g., [5–8]). In light of the KSA's vision-2030, urban development is rapidly increasing and thus, the possibility of constructing lightweight structures on expansive soils in different areas of the KSA

increases. This highlights the crucial need for practical recommendations to help civil engineers to mitigate or eliminate the potential problems and damages to lightweight structures constructed on expansive soils and consequently reduce the loss of millions of dollars.

The design strategy used to minimize the damage of lightweight structures constructed on expansive soil is to design the structure to be stiff enough to accommodate the soil movements [9–11). The two foundation systems that are successfully used in different countries in which expansive soils exist (i.e., the United States, Australia, South Africa, and the Middle East) to mitigate or eliminate the damage of lightweight structures constructed on expansive soils are stiffened raft and the inverted T-section strip footings [10–14].

Many design methods have been developed over the years for the analysis and design of the stiffened raft resting on expansive soil, such as the Lytton method [15], Walsh method [16], Mitchell method [17], Swinburne method [18], Post-Tensioning Institute method [19], Brauid method [14], and Shams et al.'s method [11]. The approach used by most of the design methods is divided into two successive stages: Stage 1 assumes a predefined distorted mound shape for two worst conditions of edge heave and edge shrinkage, and Stage 2 analyzes the interaction between the stiffened raft and the distorted mound shape to obtain the deflections and the internal forces in the stiffened raft. This research is concerned with Stage 1 (i.e., predicting the 3D free surface distorted mound shape using the climate-controlled expansive soil parameters). The climate-controlled expansive soil parameters have also been used by most of the existing design methods of stiffened rafts resting on expansive soils, such as Brauid et al.'s method (2016) and Shams et al.'s method [11].

In this research, a rational method is presented for estimating the climate-controlled expansive soil parameters from the results of the routine site geotechnical tests. These parameters include the equilibrium soil suction, the amplitude of surface suction change, the suction compression index, the diffusion coefficient of the soil, the active zone depth, and the initial and final soil suction profiles. The climate-controlled soil parameters are used as input for the program SUCH to predict the 3D distorted mound shapes. SUCH is used in a parametric study to investigate the effect of the climate-controlled parameters on the distorted mound shape underneath a flexible cover (i.e., raft) of different aspect ratios for the case of edge shrinkage.

2. Computer Program SUCH

El-Garhy et al. [20–24] have been developed a program called SUCH to calculate the 3D distorted mound shape underneath a flexible impermeable cover due to the movements in the expansive soil (shrinkage or heave). The SUCH model has been described and validated in a series of published papers. The program SUCH estimates the distorted mound shape underneath a flexible impermeable cover slab in 3D and overcomes the disadvantage which exists in all design methods of stiffened rafts that consider the distorted mound shape in 2D and analyze the raft as a beam in both two directions separately. The program SUCH using the finite difference method, FDM, to solve the suction diffusion equation in 3D to estimate the changes in soil suction within the expansive soil underneath a flexible impermeable cover with time and the associated movements (shrink or heave) due to the changes in the climatic condition. Other edge effects, such as vertical barrier, horizontal barrier, water collects in a pond, and large trees, can be considered by the program [22, 24]. The water movement in the expansive soil mass was based on Mitchell's suction diffusion equation [25] and the soil movements (shrink or heave) calculation was based on Wray's model [26].

3. Methodology and Procedure

A rational procedure is presented and discussed in this section for estimating the climate-controlled expansive soil parameters that are used for predicting the 3D surface mound shape beneath a covered area (i.e., stiffened raft). These parameters include (1) the diffusion coefficient, α, (2) the equilibrium soil suction, ψ_e, (3) the amplitude of surface suction change, ψ_o, (4) the depth of active zone, Z_α, and (5) the suction compression index, SCI. Also, a recommendation for estimating the initial state of soil suction in the expansive soil before foundation construction and the worst expected boundary conditions, which may cause the worst soil suction distribution through the expansive soil under the raft foundation during the lifetime of the structure, is presented. The proposed procedure is explained through its application to calculate the climate-controlled soil parameters for expansive soil in different locations in the KSA. However, the proposed procedure can be used at any geographical location of expansive soils around the world. The word climate in this study refers to the climatic cycles (i.e., wetting and drying cycles during the year) that control the change in soil suction (i.e., water content) at the surface boundary of the expansive soil mass.

3.1. Climate-Controlled Soil Parameters in the KSA. A review of the available technical literature pertaining to expansive soils in the KSA showed that there are no measurements for all of the climate-controlled expansive soil parameters at any site. Therefore, the properties of expansive soils that are routinely measured during the site investigation are used in an attempt to determine these parameters.

Dhowian [27] performed a detailed investigation and documentation for the characteristics of the expansive soils in the KSA. Expansive soils in the KSA mainly consist of two distinct soils (i.e., sedimentary rocks and clayey soils). Expansive sedimentary rocks include shales, claystone, and siltstones. The shales with various degrees of weathering prevail in a strip adjacent to the west boundary of the Arabian Shield. The strip starts around Al-Ghat and extends to the northwest, enclosing the Tabuk and Tayma regions. Expansive clayey soils are usually found in small areas scattered in the Arabian Shield and Arabian Shelf, such as the Madina and Hofuf regions. The properties of the silty shale and clayey shale soils have been investigated by a number of researchers (e.g., [2–7, 28–33]). The average geotechnical properties of both shale and clayey soils are presented in Table 1.

Dhowian [27] reported that based on experimental studies on the expansive soils in the KSA shown that the

Table 1: Average properties for expansive soils at different locations in the KSA.

No.	Location	Soil type	USCS group symbol	Consistency limits (%)			Suction parameters (bars)		Slope of SWRC (kPa or p^F) units	In situ water content	% Clay
				LL	PL	PI	A	B	$B = (dh/dw)$	(%)	(%)
1	Tayma	Silty shale	CL–ML	38	27	13	1.85	−0.057	−5.70	2.3	23
2	Tabuk	Clay shale	MH	61	27	34	1.61	−0.025	−2.50	4.5	45
3	Al-Ghat	Silty shale	CL	46	21	25	1.67	−0.017	−1.70	12	45
4	Al-Ghat	Clay shale	CH	65	30	35	2.1	−0.025	−2.50	19	72
5	Madina	Green clay	CH	105	39	66	2.28	−0.03	−3.00	59.1	64
6	Madina	White clay	CH	82	37	45	2.34	−0.045	−4.50	33.1	68
7	Hofuf	Calcareous clay	CH–MH	60	24	36	2.16	−0.033	−3.30	14	37

USCS, unified soil classification system; SWRC, soil–water retention curve.

relationship between the soil suction and the water content can be represented by a straight line as follows:

$$\log \psi = A - Bw, \tag{1}$$

where ψ is the soil suction in bars, w is the water content, and A, B are the intercept and the slope of the straight line. A similar linear relationship between the soil suction and the water content has been reported by others (e.g., [25, 34, 35]).

3.1.1. Estimating the Equilibrium Soil Suction. If the equilibrium soil suction, ψ_e, is not measured or known, it can be predicted by one of the following techniques: (1) the equilibrium conditions beneath the center of the covered area (i.e., stiffened raft or pavement) or at the bottom of the active zone depth will occur when the ratio of the water content to the plastic limit, w_e/PL, reaches a constant value less than 1.0 for arid climate areas [36]. Once the ratio of w_e/PL is known, the equilibrium water content is calculated from the plastic limit, and the corresponding equilibrium soil suction can be determined from the suction-water content relationship or the soil–water retention curve (SWRC), and (2) the equilibrium soil suction can also be calculated from the Thornthwaite Moisture Index (TMI) if it is estimated or known. The TMI is a dimensionless index varying from +100 to −100, representing the climate conditions. A positive value of TMI indicates an average annual runoff, whereas a negative value denotes water deficiency. The TMI is an important parameter to calculate the equilibrium soil suction and the active zone depth [37, 38]. Relationships between the equilibrium soil suction and the TMI have been presented in the literature [19, 38, 39]. The relationship of Russam and Coleman [39] for three soil types, including heavy clay is shown in Figure 1. Vann and Houston [38] improved the relationship between the TMI and the equilibrium soil suction using more measured soil suction data and provided the following fitting equation to calculate ψ_e in p^F unit.

$$\psi_e = 0.00002(\mathrm{TMI})^2 - 0.0053(\mathrm{TMI}) + 3.9771. \tag{2}$$

The first technique is used here to calculate the equilibrium soil suction using the equilibrium ratio, w_e/PL, of 0.75

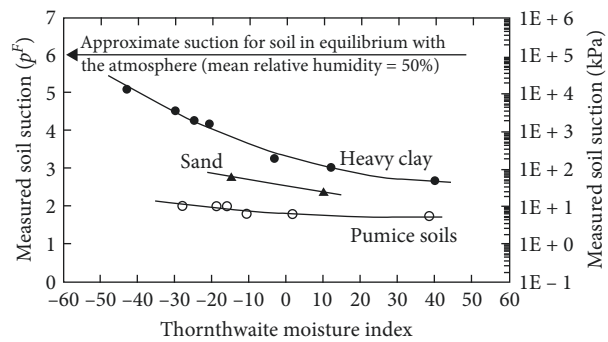

Figure 1: Variation of soil suction of road subgrade with TMI [39].

[23]. The measured plastic limits and the parameters of the suction-water content relationship (i.e., A and B) presented in Table 1 are used to calculate the equilibrium water content, w_e, and the corresponding equilibrium soil suction from Equation (1) for expansive soils at different locations in the KSA, as shown in Table 2.

3.1.2. Estimating the Amplitude of Surface Suction Change. The amplitude of surface suction change, ψ_o, is defined as the difference between the equilibrium soil suction beneath the covered area and the free field surface soil suction around the covered area. The free field soil suction is dependent on the climatic conditions; the maximum value occurs in summer (dry soil), and the minimum value occurs in winter (saturated soil). The minimum soil suction at the saturated condition of the soil is taken 2.0 p^F by Lytton [35]. Based on experimental works, Cameron [40] reported that the maximum soil suction value of 6.8 p^F for dry soil is true for some Australian soils, but it cannot be a universally accepted value for all soils. It was pointed out that the soil suction for dry soil reaches a maximum value of 7 p^F [35, 41–43]. Therefore, soil suction for dry soil should be verified for each soil type. Several of the existing methods have recommended the value of 2.0 p^F for the amplitude of surface suction change [14]. AS2870 [37] recommended the value of U_o varies from 1.2 to 1.5 p^F for different locations in Australia. The ψ_o is considered one of the parameters controlling the moisture diffusion and the volume changes (shrink/heave) in expansive soil under the covered area.

Table 2: Calculated w_e, ψ_e, ψ_o, and TMI for expansive soils at different locations in the KSA.

No.	Location	w_e (%)	ψ_e from Equation (1) (bars)	ψ_e (kPa)	ψ_e (p^F)	ψ_o (p^F)	ψ_o (kPa)	TMI from Figure 1 at ψ_e
1	Tayma	20.25	4.97	497	3.70	1.70	5.01	−15.00
2	Tabuk	20.25	12.71	1,271	4.10	1.90	7.94	−21.00
3	Al-Ghat	15.75	24.55	2,455	4.39	1.61	4.07	−27.80
4	Al-Ghat	22.50	31.62	3,162	4.50	1.50	3.16	−30.00
5	Madina	29.25	25.29	2,529	4.40	1.60	3.98	−28.00
6	Madina	27.75	12.33	1,233	4.09	1.91	8.13	−14.50
7	Hofuf	18.00	36.81	3,681	4.57	1.43	2.69	−31.60

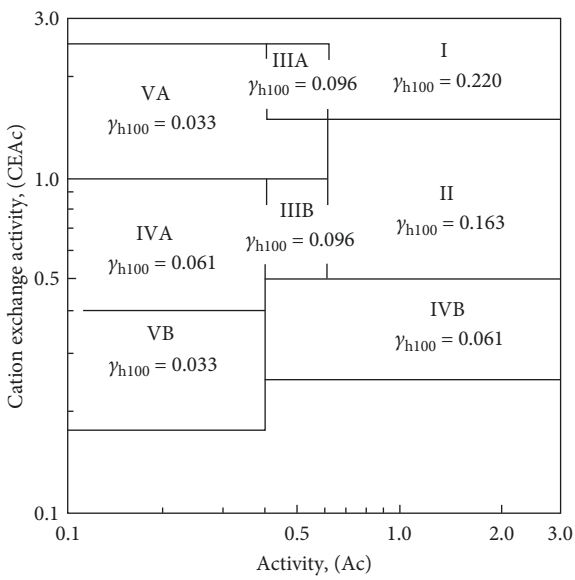

Figure 2: Chart for calculating SCI [45].

In the present analysis, the amplitude of surface suction change, ψ_o, can be considered the minimum of $(6.0 - \psi_e)$ or $(\psi_e - 2.0)$ [23] and is calculated for the different locations in the KSA, as shown in Table 2.

3.1.3. Estimating the Suction Compression Index. McKeen [44] developed a chart to determine the SCI, as shown in Figure 2. The chart is divided into mineralogical groups according to clay activity, $A_c = \mathrm{PI}/\%\,\mathrm{Clay}$, and the cation exchange activity, $\mathrm{CEAc} = \mathrm{CEC}/\%\,\mathrm{Clay}$. The soil properties necessary to use the chart are the plasticity index, PI, the percentage of clay (i.e., the percentage of the total soil sample passing through No 200 sieve), and the cation exchange capacity of the soil, CEC. The cation exchange capacity, if not measured, can be calculated with a satisfactory accuracy from the plastic limit, $\mathrm{CEC} = (\mathrm{PL})^{1.17}$ [26, 35, 45].

The values of SCI shown on the chart correspond to SCI of soil with 100% clay content. Therefore, the actual value of SCI is proportional to the actual percent of clay in the soil, $\mathrm{SCI} = \mathrm{SCI}_{\mathrm{chart}}(\%\,\mathrm{Clay})$.

The SCI can also be determined by two more regression equations reported in the literature, Equation (3), which is dependent on the slope of the SWRC [46], and Equation (4), which is the improved version of Equation (3) [47]. The slope of the SWRC is different in the drying and wetting paths [48, 49]. Therefore, it is recommended to use the slope of the wetting SWRC in the calculation of the soil heave and the slope of the drying SWRC in the calculation of the soil shrinkage to estimate the SCI.

$$\mathrm{SCI} = -0.02673\left(\frac{d\psi}{dw}\right) - 0.38704, \tag{3}$$

$$\mathrm{SCI} = -10\left(\frac{d\psi}{dw}\right)^{-2}, \tag{4}$$

where $d\psi/dw$ is a negative value defined as the slope of the SWRC (i.e., the relationship between soil suction in p^F unit and the gravimetric water content as a percentage). It is important to note that the SCI value calculated from Equations (3) and (4) is negative.

3.1.4. Estimating the Diffusion Coefficient. Jayatilaka and Lytton [50] developed an empirical equation relating the field diffusion coefficient, α, to the slope of the SWRC, S, and the suction compression index, SCI.

$$\alpha = 0.0029 - 0.000162(S) - 0.0122\,(\mathrm{SCI}). \tag{5}$$

Lytton et al. [51] reported that Equation (5) takes into account the cracks present in the soil mass in the field, and therefore, the diffusion coefficient obtained by Equation (5) is higher than that measured in the laboratory for intact soil specimens. McKeen and Johnson [45] reported that the soil diffusion coefficient of the cracked soils varies from 1×10^{-4} to $4.2 \times 10^{-4}\,\mathrm{cm}^2/\mathrm{s}$ in the field for various fine-grained soils. Mabirizi and Bulut [52] measured the wetting diffusion coefficients of nine soil specimens from Oklahoma and found that the diffusion coefficient of a soil specimen with a significant crack was $5.3 \times 10^{-4}\,\mathrm{cm}^2/\mathrm{s}$, whereas the diffusion coefficients of several intact (uncracked) soil specimens were approximately $0.5 \times 10^{-4}\,\mathrm{cm}^2/\mathrm{s}$ (i.e., the measured diffusion coefficient of the cracked soil specimens is approximately 10 times larger than the diffusion coefficient of the intact soil specimen). Based on a numerical analysis, Chen and Bulut [53] concluded that the ratio of the cracked soil diffusion coefficient over the intact one is from several times to

Table 3: Calculated SCI, α, and Z_a, for the expansive soils at different locations in the KSA.

No.	Location	A_c	CEAc	SCI from Figure 2	α from Equation (5) (cm^2/s)	Z_a (m) from Equation (7) $\Delta\psi_{max}$ 0.1 (p^F)	0.05 (p^F)	0.01 (p^F)
1	Tayma	0.57	2.06	0.008	3.731E − 03	3.28	3.93	5.43
2	Tabuk	0.76	1.05	0.073	2.410E − 03	2.72	3.24	4.45
3	Al-Ghat	0.56	0.78	0.043	2.648E − 03	2.72	3.27	4.53
4	Al-Ghat	0.49	0.74	0.069	2.462E − 03	2.57	3.10	4.31
5	Madina	1.03	1.14	0.104	2.113E − 03	2.43	2.91	4.04
6	Madina	0.66	1.01	0.111	2.277E − 03	2.65	3.15	4.32
7	Hofuf	0.97	1.11	0.060	2.699E − 03	2.66	3.20	4.48

several tens of times when the intact diffusion coefficient is in the order of $10^{-5}\,cm^2/s$, whereas it can reach several hundreds or thousands of times when the intact soil diffusion coefficient is in the order of $10^{-6}\,cm^2/s$.

The parameter S in Equation (5) is a negative value (equal to $d\psi/dw$), and if the measurements of the soil suction are not available, the S value can be empirically estimated from the Liquid limit, the plasticity index, and the percentage of the clay content (% Clay).

$$S = -20.29 + 0.1555\,(\mathrm{LL\%}) - 0.117\,(\mathrm{PI\%}) + 0.0684\,(\%\,\mathrm{Clay}). \tag{6}$$

Thakur [54] reported that the S values estimated from Equation (6) are in reasonable agreement with those obtained from the laboratory curves.

In the present analysis, Equation (5) is used to calculate the diffusion coefficient of the expansive soils at different locations in the KSA, and the results are presented in Table 3.

3.1.5. Estimating the Active Zone Depth. The active zone depth, Z_α is estimated from the equation proposed by McKeen and Johnson [45], Equation (7), in which the active zone depth is a function of the amplitude of surface suction change, the frequency number, the diffusion coefficient of the soil, and the maximum suction change below which the soil movements is considered insignificant. Equation (7) has been recommended to calculate the active zone depth by researchers (e.g., [22, 55]).

$$Z_a = \frac{\ln\left(\frac{2\psi_o}{\Delta\psi_{max}}\right)}{\sqrt{\frac{n\pi}{\alpha}}}, \tag{7}$$

where ψ_o is the amplitude of surface suction change (p^F), n is the frequency number (cycles/year), α is the field diffusion coefficient of the soil (cm^2/s), and $\Delta\psi_{max}$ is the maximum suction change. The frequency number, n, is defined as the number of cycles of wetting and drying that occur during the year. A small n value means wetting or drying occurs over a longer time interval.

For design purposes, the n value is taken 0.5 as recommended by McKeen and Johnson [45], and the value of $\Delta\psi_{max}$ is taken $\leq 0.1\,p^F$ [22, 55]. The calculated active zone depths by Equation (7) for the different locations of the expansive soils in the KSA at different values of $\Delta\psi_{max}$ are presented in Table 3. As illustrated in Table 3, the smaller the value of $\Delta\psi_{max}$, the greater the active zone depth.

3.1.6. Initial and Final Soil Suction Profiles. To estimate the distortion mound shape by the SUCH program, the user has to input the initial suction condition within the expansive soil under the raft and the most severe expected environmental boundary conditions, which may cause the greatest difference in soil suction throughout the active zone depth. The field soil suction profile just before the building construction is considered to provide the initial soil suction. Field measurements or laboratory measurements from undisturbed soil samples taken at different depths can determine the initial suction values. If soil suction measurements are not available, the steady state initial soil suction profile (i.e., driest, wettest, or equilibrium profile) can be predicted using the suction diffusion equation [25].

In the design of stiffened rafts, two types of distortion mound shapes of expansive soils (i.e., edge heave and edge shrinkage) are considered to produce the maximum values of the internal forces and deflections [56], Braiud et al. 2016, [11]. Wray [26] pointed out that both severe climatic conditions of extended drought and extended wet must be considered in the design of a stiffened raft because it is impossible to know if the raft will be subjected to one or both of these severe conditions.

In the present study, the distortion mode of edge shrinkage is simulated by a 4-month dry spell following an equilibrium suction condition under the raft, and the distortion mode of edge heave is simulated by a 4-month wet spell following an equilibrium suction condition in the soil under the raft. The time of 4 months was found enough to predict the dry and wet suction distribution through the expansive soil for the two cases of extended draught and extended wet for expansive soils in the KSA. The boundary values of the free surface soil suction outside the domain of the covered area (i.e., stiffened raft) are assumed to be 6.0 and 2.0 p^F for dry and saturated soils, respectively [26].

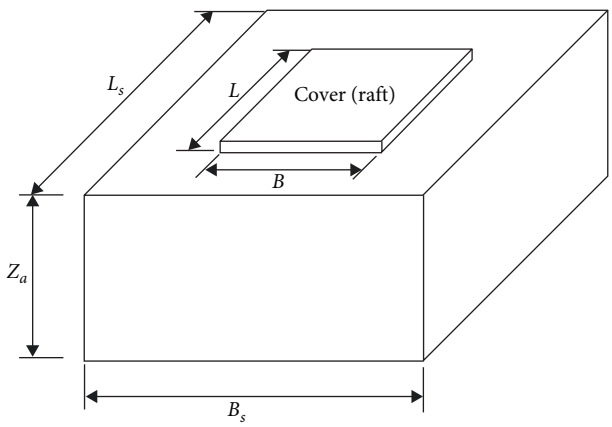

FIGURE 3: Dimensions of the flexible impermeable cover and the soil mass.

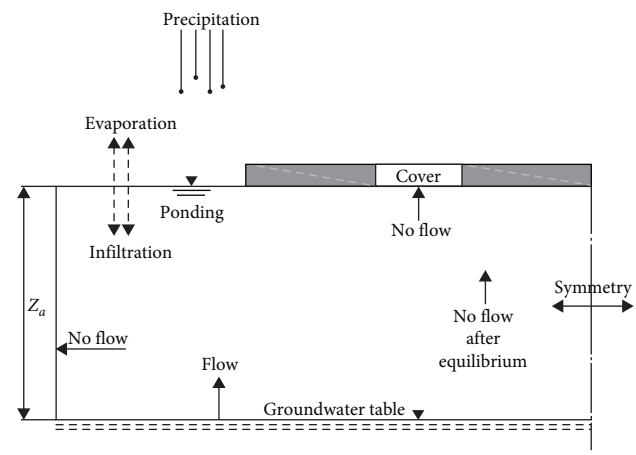

FIGURE 4: Various types of boundary conditions considered in the program SUCH [22].

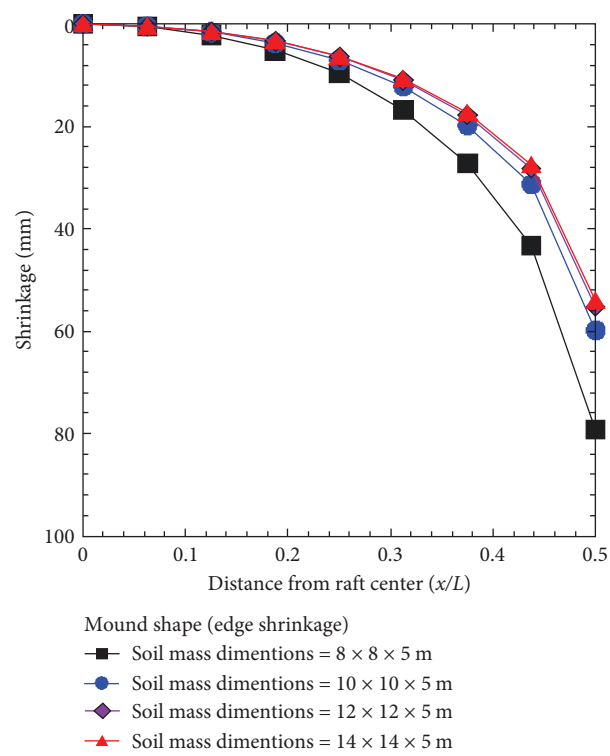

FIGURE 5: Effect of the soil mass dimensions on the soil movements along the y-axis of the covered area (8×8 m).

4. Parametric Study

The realistic mound shape predicted by SUCH that would be formed beneath a flexible cove slab in the two cases of edge heave and edge shrinkage depends on the interaction between the climate and the expansive soil. The parameters that affect the distorted mound shape include the amplitude of surface suction change, ψ_o, the equilibrium soil suction, ψ_e, the active zone depth, Z_a, the diffusion coefficient of the soil, α, the suction compression index, SCI, the initial soil suction within the soil, the boundary conditions of surface soil suction outside the domain of the covered area, and the dimensions of the covered area (i.e., dimensions of the raft).

First, the effect of the soil mass dimensions under the flexible impermeable cover shown in Figure 3 on the distorted mound shape for the case of edge shrinkage is investigated to select the optimal dimensions of the soil mass to use in the present study. The soil mass is discretized into a grid of nodes to apply the FDM to solve the 3D suction diffusion equation to obtain the changes in suction within the expansive soil and the associated movements due to different surface boundary conditions. Boundary values or boundary gradients can be used to express any of the engineering boundary conditions. El-Garhy and Wray [22] describe a series of typical common problems that result in a change in suction in expansive soils and various types of boundary conditions, as illustrated in Figure 4. Three rafts of sizes 8×8 m, 8×12 m, and 16×28 m are studied, and four soil masses of different dimensions under each raft are considered. In all the studied cases, the advantage of symmetry is considered, and the values of the input parameters are $\alpha = 0.07776\,\mathrm{m}^2/\mathrm{day}$, $\mathrm{SCI} = 0.02$, $\psi_e = 4.0\,p^F$, $Z_a = 5.0$ m, $\psi_o = 2.0\,p^F$.

Figures 5–7 show the effect of the soil mass dimensions on the mound shape represented by the soil movements along the y-axis for the different covered area dimensions. As illustrated in Figures 5–7 for the covered areas 8×8 m, 8×12 m, and 16×28 m the soil movements along the y-axis for the soil masses of 12×12 m, 12×16 m, and 24×36 m, respectively, are identical with the soil movements along the y-axis for the soil masses of larger dimensions. Therefore, it is quite enough, in the present study, to consider a limited soil region around the perimeter of the raft equal to or greater than the one-fourth width of the raft.

The existing design methods of slab foundations resting on expansive soil assume the interaction to be between the slab foundation and an already distorted mound shape (i.e., center lift or edge lift) and require an estimation of the initial distorted mound shape. The initial distorted mound shape is defined by the edge moisture variation distance, e_m, and the maximum differential movement, y_m.

The effect of the different parameters on the distorted mound shape is investigated for a cover (i.e., raft) of different

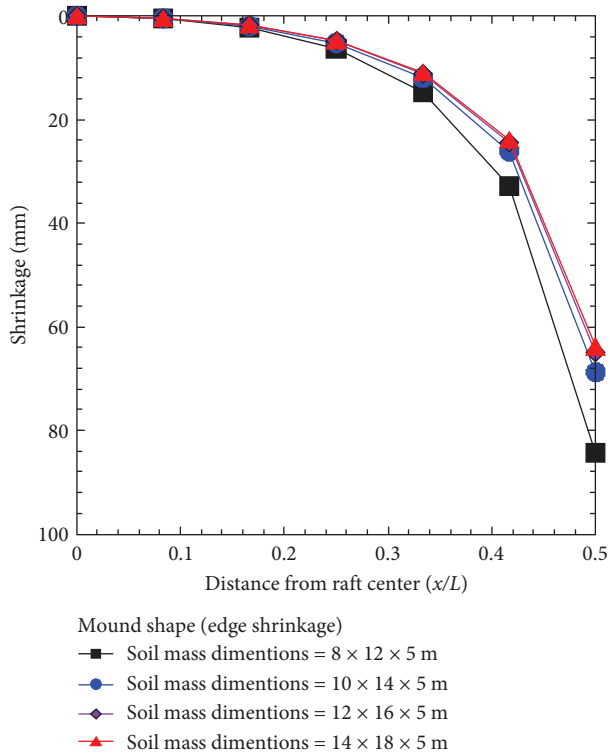

Figure 6: Effect of the soil mass dimensions on the soil movement along the y-axis of the covered area (8×12 m).

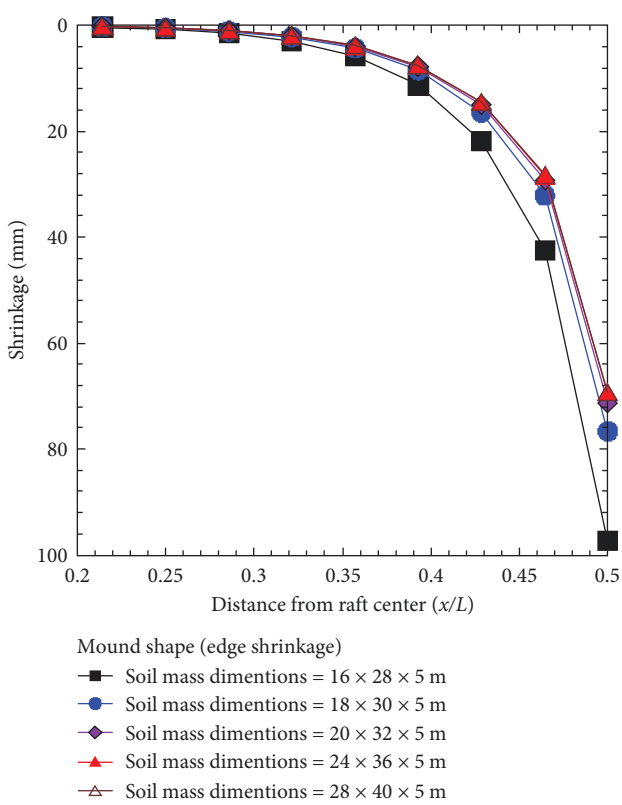

Figure 7: Effect of the soil mass dimensions on the soil movement along the y-axis of the covered area (16×28 m).

Table 4: Range of the parameters for the parametric study.

Z_a(m)	$\psi_e p^F$(kPa)	$\psi_o p^F$(kPa)	α(m^2/day)	SCI
1.0	2.5 (31.623)	0.5 (0.316)	0.07776	0.005
2.0	3.0 (100.000)	1.0 (1.000)	0.02592	0.010
3.0	3.5 (316.228)	1.5 (3.162)	0.00864	0.020
4.0	3.75 (562.341)	1.75 (5.623)	0.00259	0.030
5.0	4.0 (1000)	2.0 (10.000)	0.000864	0.040

dimensions. The studied raft dimensions are 8×8 m, 12×16 m, 16×28 m, and 20×40 m, which represents different aspect ratio, L/B, of 1.0, 1.33, 1.75, 2.0. The values of the investigated parameters are shown in Table 4.

The parameters are selected to cover the range of the climate-controlled parameters for the expansive soils at different locations in the KSA presented in Tables 2 and 3. In the parametric study, only one parameter is changed, and all other parameters are kept constant at the maximum values, according to Table 4.

4.1. Effect on the Shape of the Distorted Mound. Figures 8–11 show the effect of the climate-controlled parameters and the dimensions of the cover, L/B, on the shape of the distorted mound represented by the soil movement, y/y_m, along the y-axis of the studied covered slabs. For all the climate-controlled parameters, the increase in the L/B ratio of the cover results in an increase in the flatter intermediate area of the distorted mound; in other words, the initial contact area between the distorted mound and the cover increases, as shown in Figures 8–11. The initial contact area is considered an important parameter in the analysis of the interaction between stiffened rafts and the distorted mound of the expansive soil ([11]). For each L/B ratio, the increase in the diffusion coefficient or the active zone depth causes a decrease in the intermediate flatter area of the distorted mound, as shown in Figures 8 and 11, whereas there are no effects for the increase in the suction compression index or the amplitude of surface suction change on the shape of the distorted mound, as shown in Figures 9 and 10.

4.2. Effect on the Maximum Differential Movement. The effect of the different parameters on the maximum differential movement, y_m, for rafts (i.e., covers) of different aspect ratios is investigated. Figures 12–15 show the effect of the climate-controlled parameters on the y_m/B of the edge shrinkage mound shape for different cover aspect ratios. As illustrated in Figures 12–15, the following findings may be observed: (1) the y_m increases nonlinearly as the diffusion coefficient and the active zone depth increase for all the studied covers of different aspect ratios, as shown in Figures 12 and 15, respectively, (2) the y_m increases linearly as the suction compression index and the amplitude of surface suction change increase for all the studied covers of different aspect ratios, as shown in Figures 13 and 14, (3) as the diffusion coefficient increases the rate of increase in

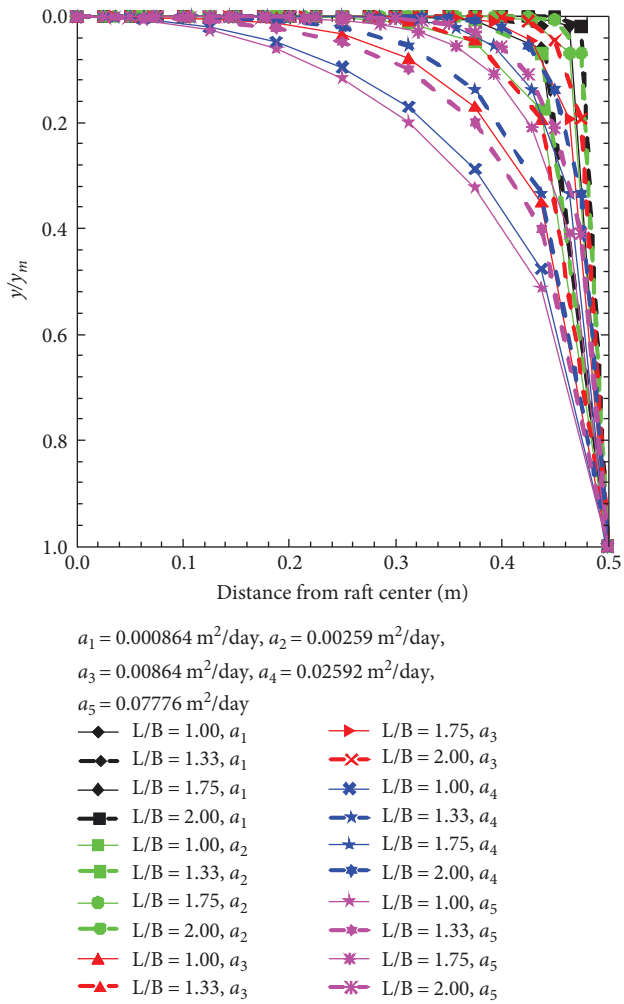

FIGURE 8: Effect of the diffusion coefficient on the shape of the mound shape underneath a flexible cover slab of different aspect ratios (SCI = 0.04, $U_e = 4p^F, \psi_o = 2.0\ p^F, Z_a = 5.0$ m).

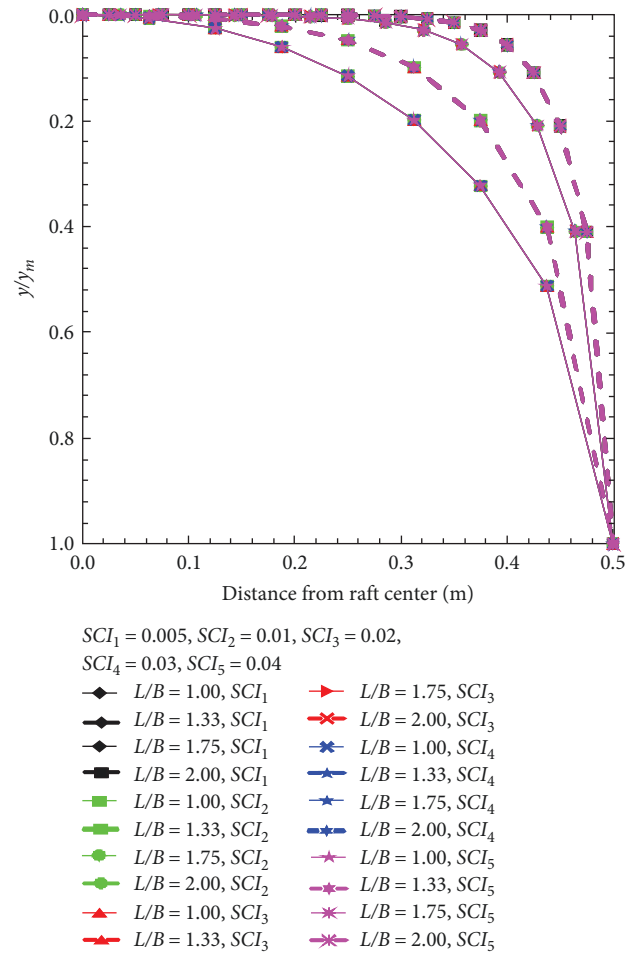

FIGURE 9: Effect of the suction compression index on the mound shape underneath a flexible cover slab of different aspect ratios ($\alpha = 0.07776$ m^2/day, $U_e = 4p^F, U_o = 2.0\ p^F, Z_a = 5.0$ m).

the y_m decreases up to a certain value after which the y_m reached a constant value.

4.3. Effect on the Edge Moisture Variation Distance. The reliable determination of the edge moisture variation distance or the edge distance, e_m, is regarded as a major concern [35]. The different methods of calculating the edge moisture variation distance have been presented, discussed, and compared by El-Garhy and Wray [22]. The magnitude of the edge moisture variation distance, sometimes called the edge penetration distance or the edge distance, depends mainly on the climate-controlled parameters and the climatic conditions.

The results of the parametric study were used to investigate the effect of the different climate-controlled parameters and the dimensions of the covered area (i.e., raft dimensions) on the edge moisture variation distance, e_m. The e_m is determined from the predicted mound shape as the distance from the edge of the raft to the point at which the soil movement, y, is equal to $0.05y_m$ (where y_m is the maximum differential mound movement at raft mid edge point) along the x-axis (i.e., short direction) and y-axis (i.e., long direction) of the covered area, as shown in Figure 15.

Based on this definition, the values of e_{mx} and e_{my} in the x and y directions were calculated and compiled. A sample of results is displayed in Table 5 for the effect of the diffusion coefficient and the aspect ratio of the raft, L/B, on the e_{mx} and e_{my} in the x and y directions. Similar three tables for the effect of the other climate-controlled parameters (i.e., Z_a, ψ_o, and SCI) are obtained but not included for space limitation.

Figures 16–19 show the effect of the climate-controlled parameters on the e_m/B for rafts of different aspect ratios. Referring to simulation results and Figures 16–19, it is observed that (1) the absolute value of e_m, as identified in Figure 20, is approximately equal in the x and y directions (i.e., $e_{mx} = e_{my} = e_m$), as shown in Table 5 for each raft, (2) the e_m/B increases nonlinearly as the α and the Z_a increase for rafts of different aspect ratios, as shown in Figures 16 and 19, (3) changes in the ψ_0 as well as the changes in the SCI have no effect in the e_m/B for each L/B ratio, (4) at a specified value for each of the climate-controlled parameters (i.e., α, Z_a, ψ_o, and SCI) the value of e_m/B increases as the raft

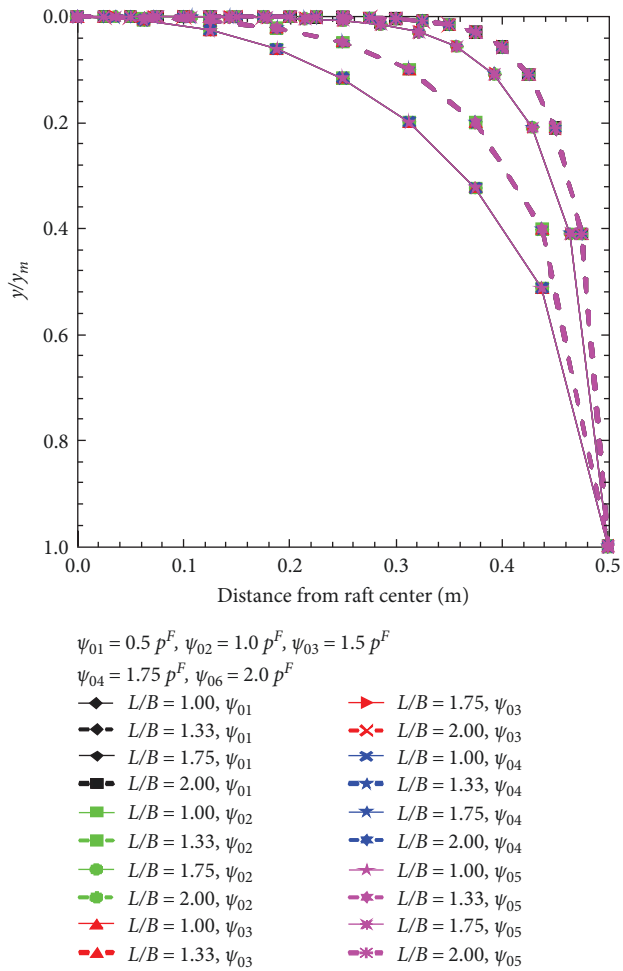

FIGURE 10: Effect of the amplitude of surface suction change on the mound shape underneath a flexible cover slab of different aspect ratios ($\alpha = 0.07776\ \mathrm{m}^2/\mathrm{day}$, $U_e = 4p^F$, SCI = 0.04, $Z_a = 5.0$ m).

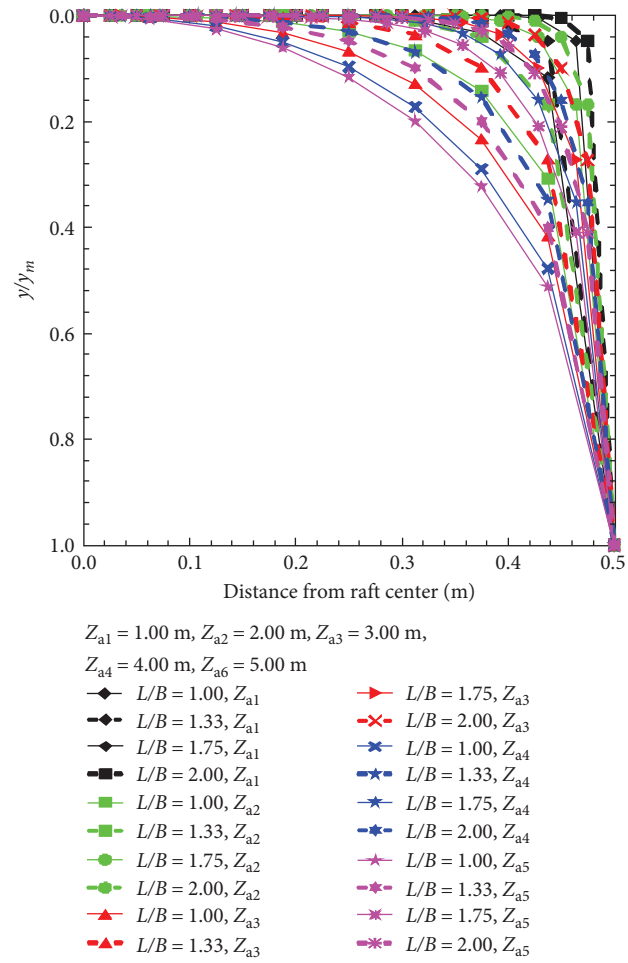

FIGURE 11: Effect of the active zone depth on the mound shape underneath a flexible cover slab of different aspect ratios ($\alpha = 0.07776\ \mathrm{m}^2/\mathrm{day}$, $U_e = 4p^F$, SCI = 0.04, $U_o = 2.0\ p^F$).

aspect ratio decreases for as shown in Figures 16–19 (e.g., at the SCI = 0.02, the value of $e_m/B = 0.19$ at $L/B = 2.0$ and the value of $e_m/B = 0.31$ at $L/B = 1.0$).

4.3.1. Equations to Calculate the Edge Distance. Multiple regression analysis is used to express the value of e_m as a function of five independent variables; these are α, Z_a, ψ_o, SCI, and L/B. It is found that expressing the e_m in the form of a dimensionless form yields simpler expressions and more accurate predictions of the value of e_m. Therefore, e_m is expressed in its dimensionless form e_m/B. Several multiple regression models were attempted to obtain an expression of e_m/B. It was found that the value of e_m/B is well-represented by the following:

$$\frac{e_m}{B} = 1.03\alpha^* + 0.914Z_a^* + 0.0464\,\mathrm{SCI} + 0.00217\psi_o + 0.101\left(\frac{L}{B}\right) - 0.351, \tag{8}$$

where

$$\alpha^* = a_x\left(1 - e^{-\alpha b_x}\right),\ a_x = 0.334 - 0.09\left(\frac{L}{B}\right),$$
$$b_x = 103.64\left(\frac{L}{B}\right)^{-1.303},\ Z_a^* = a_z(Z_a)^{b_z}, \tag{9}$$
$$a_z = 0.302e^{-0.864\left(\frac{L}{B}\right)},\ \text{and}\ b_z = 1 - \mathrm{e}^{-0.92\left(\frac{L}{B}\right)}.$$

In the equation, α is in $\mathrm{m}^2/\mathrm{day}$, Z_a, L and B in m, and ψ_o in p^F. The comparison of predicted values of e_m/B, $(e_m/B)_{pr}$ versus the corresponding values from simulations, $(e_m/B)_M$, is shown in Figure 21.

For practical purposes, a simpler and equally accurate form of Equation (8) was obtained as follows:

$$\frac{e_m}{B} = 1.024\alpha^* + 0.908Z_a^* + 0.0994\left(\frac{L}{B}\right) - 0.341, \tag{10}$$

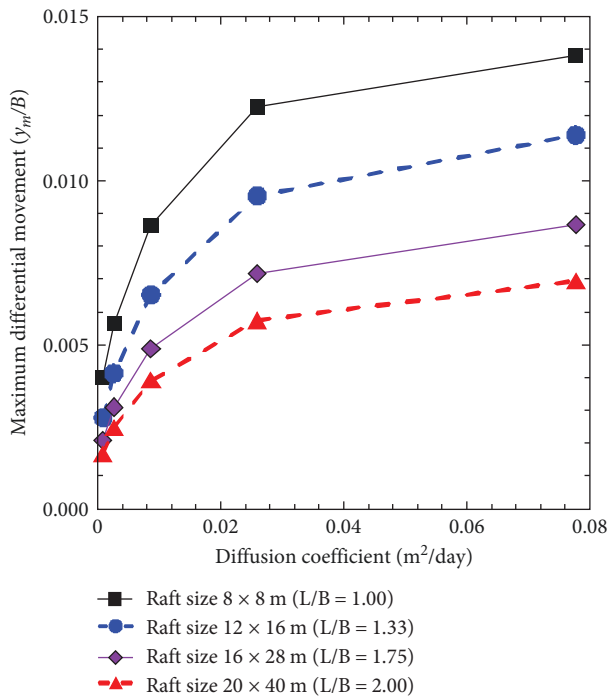

FIGURE 12: Effect of the diffusion coefficient on the maximum differential movement for rafts of different aspect ratios.

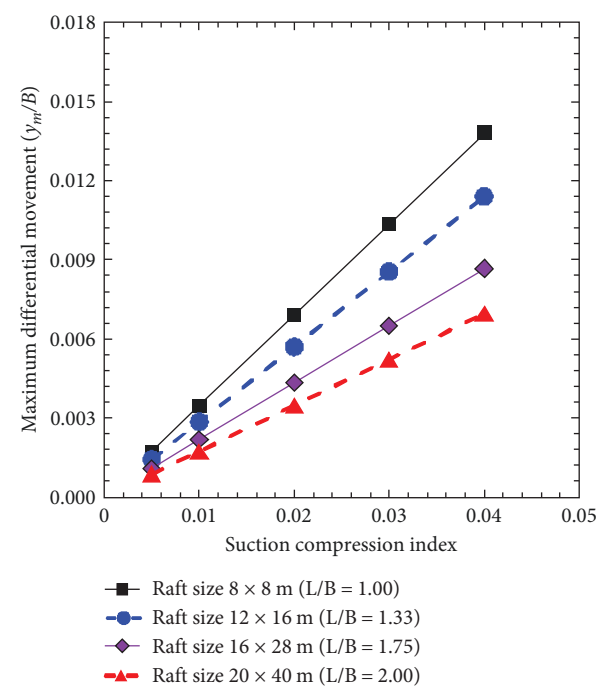

FIGURE 13: Effect of the suction compression index on the maximum differential movement for rafts of different aspect ratios.

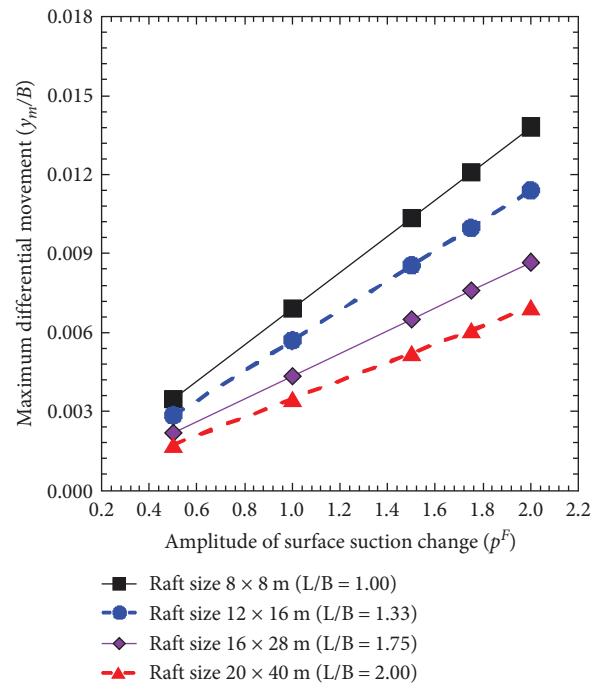

FIGURE 14: Effect of the amplitude of surface suction change on the maximum differential movement for rafts of different aspect ratios.

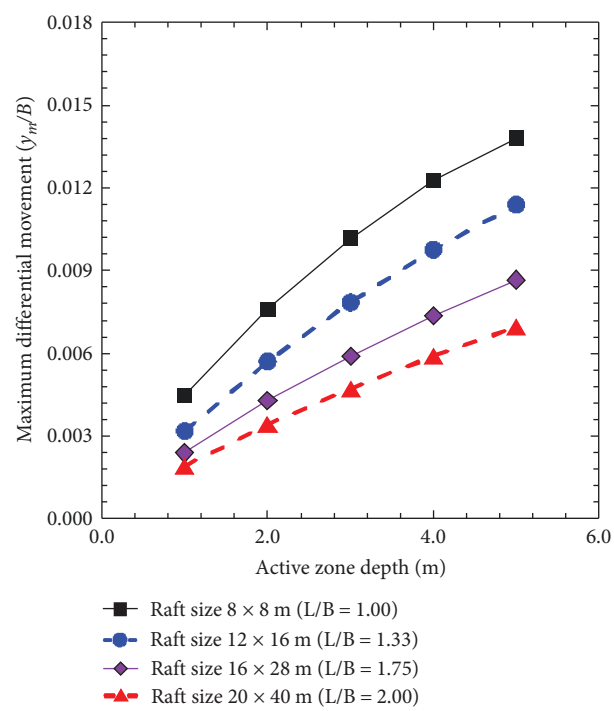

FIGURE 15: Effect of the active zone depth on the maximum differential movement for rafts of different aspect ratios.

where all the relevant parameters in Equation (10) are calculated as in Equation (8).

The comparison of predicted values of e_m/B, $(e_m/B)_{pr}$, obtained from Equation (10) versus the corresponding values from simulations, $(e_m/B)_M$, is shown in Figure 22. As shown in Figures 21 and 22, both equations (i.e., Equations (8) and (10)) yield comparable precise predictions of e_m/B, mostly within the $\pm 10\%$ of values obtained from simulations.

A comparison of Equations (8) and (10) in terms of number of independent variables and accuracy of predictions is summarized in Table 6. As shown in Table 6, even though the number of independent variables in Equation (10) is less

Table 5: Effect of α on the edge distance e_{mx} and e_{my} at different raft aspect ratios.

$\alpha(m^2/\text{day})$	e_{mx}/B	e_{mx} (m)	e_{my}/L	e_{my} (m)	L/B	e_{mx}/e_{my}
0.000864	0.07	0.568	0.07	0.568	1.00	1.00
0.00259	0.12	0.968	0.12	0.968	1.00	1.00
0.00864	0.21	1.694	0.21	1.694	1.00	1.00
0.02592	0.29	2.329	0.29	2.329	1.00	1.00
0.07776	0.31	2.454	0.31	2.454	1.00	1.00
0.000864	0.08	0.967	0.06	0.967	1.33	1.00
0.00259	0.11	1.261	0.08	1.261	1.33	1.00
0.00864	0.16	1.917	0.12	1.917	1.33	1.00
0.02592	0.24	2.875	0.18	2.917	1.33	1.02
0.07776	0.28	3.393	0.23	3.714	1.33	1.09
0.000864	0.06	0.967	0.03	0.967	1.75	1.00
0.00259	0.08	1.261	0.05	1.261	1.75	1.00
0.00864	0.12	1.917	0.07	1.917	1.75	1.00
0.02592	0.19	2.987	0.11	2.990	1.75	1.00
0.07776	0.23	3.758	0.14	3.870	1.75	1.03
0.000864	0.05	0.967	0.02	0.967	2.00	1.00
0.00259	0.06	1.261	0.03	1.261	2.00	1.00
0.00864	0.10	1.917	0.05	1.917	2.00	1.00
0.02592	0.15	2.926	0.07	2.926	2.00	1.00
0.07776	0.19	3.857	0.10	3.882	2.00	1.01

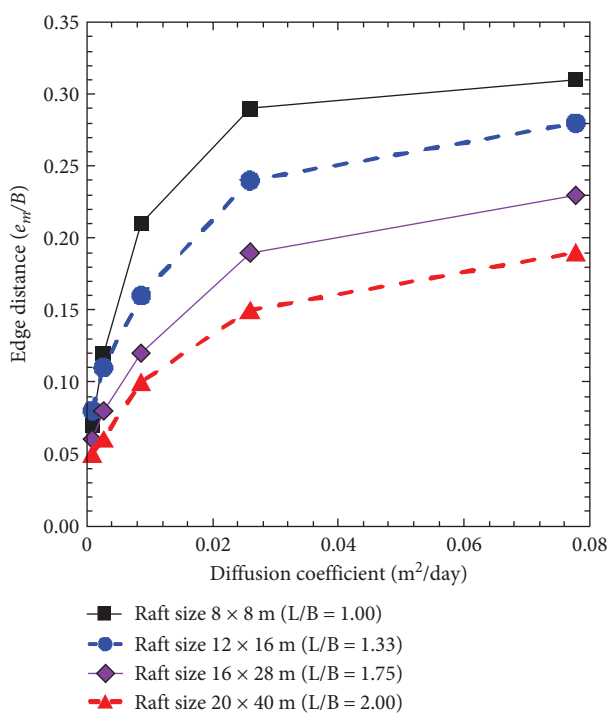

Figure 16: Effect of the diffusion coefficient on the edge distance, e_m/B, for rafts of different aspect ratios.

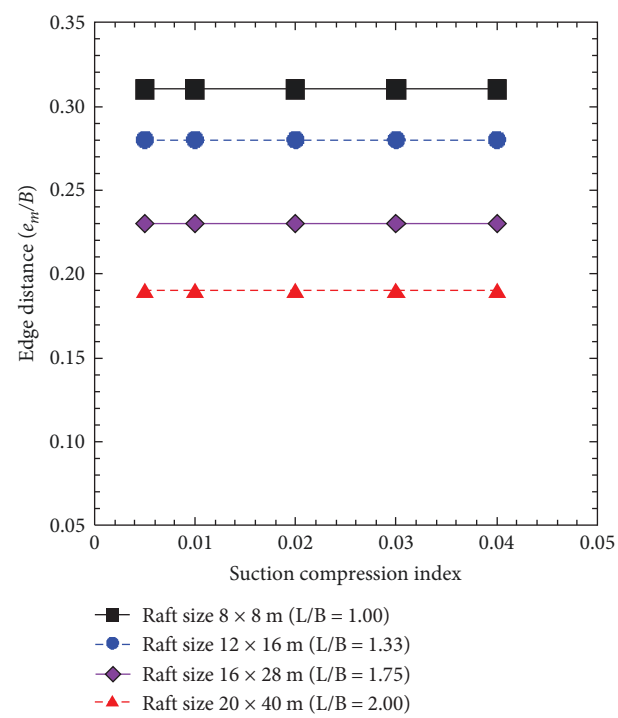

Figure 17: Effect of the suction compression index on the edge distance, e_m/B, for rafts of different aspect ratios.

than those in Equation (8), both equations have the same values of the coefficient of determination, R^2, adjusted R^2, and yield comparable precise predictions. Both equations have the same value of root mean square error, RMSE. This implies that Equation (10) is more mathematically convenient than Equation (8). This can be attributed to the fact that Equation (10) includes the significant independent variables with the largest effect on the value of e_m, namely α, Z_a, and L/B.

For the purpose of checking the accuracy of Equations (8) and (10) in estimating the edge distance, the program SUCH

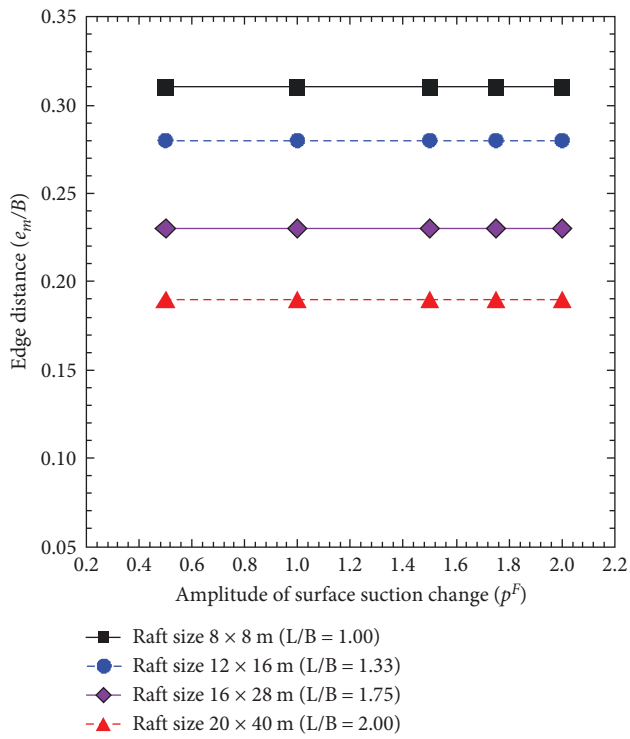

Figure 18: Effect of the amplitude of surface suction change on the edge distance, e_m/B, for rafts of different aspect ratios.

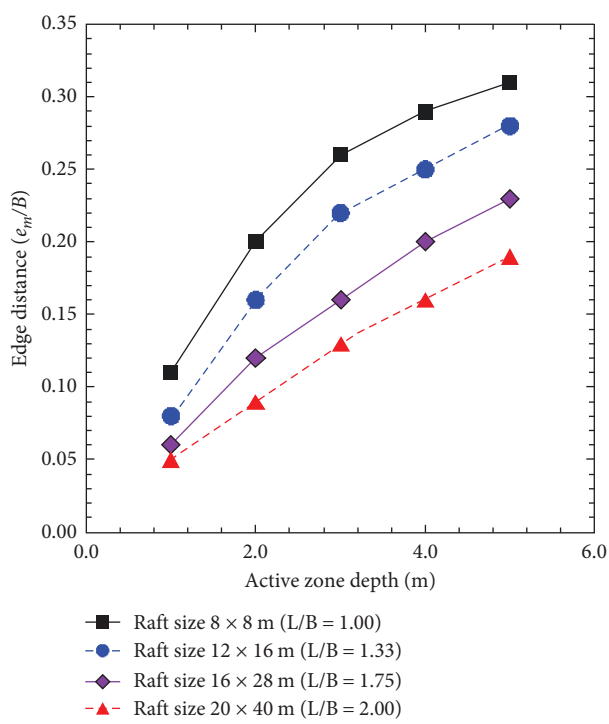

Figure 19: Effect of the active zone depth on the edge distance, e_m/B, for rafts of different aspect ratios.

was used to estimate the values of e_m for three rafts. The dimensions of the rafts were selected to cover various aspect ratios. These included 16×20 m, 16×24 m, and 20×36 m

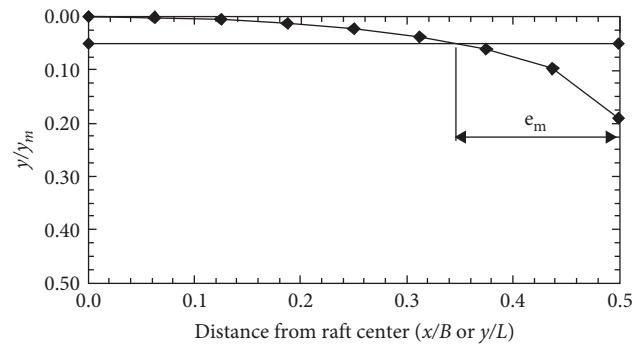

Figure 20: Definition of unsupported edge distance.

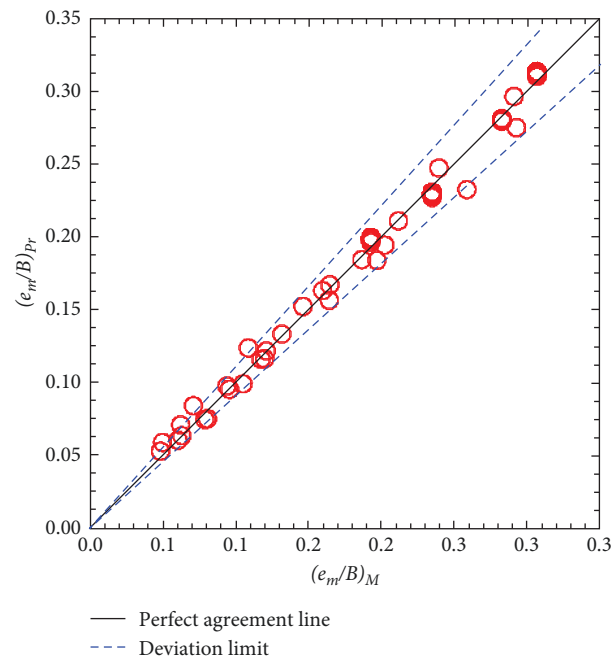

Figure 21: Comparison of $(e_m/B)_{pr}$ obtained from Equation (8) versus $(e_m/B)_M$.

rafts, which are different from raft dimensions used in the derivation of Equations (8) and (10). The values of the climate-controlled parameters are $Z_a = 4.0$ m, $\psi_e = 4.0\,p^F$, $\psi_o = 2.0\,p^F$, SCI = 0.03, and $\alpha = 0.005, 0.01, .05, 0.1\ \mathrm{m^2/day}$ were adopted in the SUCH simulations. Due to their simplicity, Equations (8) and (10) were incorporated into an Excel sheet for fast and accurate calculations. Figures 23–25 show the comparison between the values of the edge moisture variation distance obtained from the SUCH, Equations (8) and (10).

The inspection of Figures 23–25 show that (1) the values of e_m obtained by Equations (8) and (10) are comparable to their values calculated using SUCH for all the studied cases, (2) at the lower value of the diffusion coefficient (i.e., $\alpha = 0.005\ \mathrm{m^2/day}$), the predicted e_m by Equation (8) or Equation (10) is smaller than that estimated by the program SUCH by about 13.5%, 36.8%, and 40.6% for the 3-studied rafts, respectively, (3) at the higher value of the diffusion coefficient (i.e., $\alpha = 0.1\ \mathrm{m^2/day}$), the predicted e_m by Equation (8) or Equation (10) is slightly greater than that

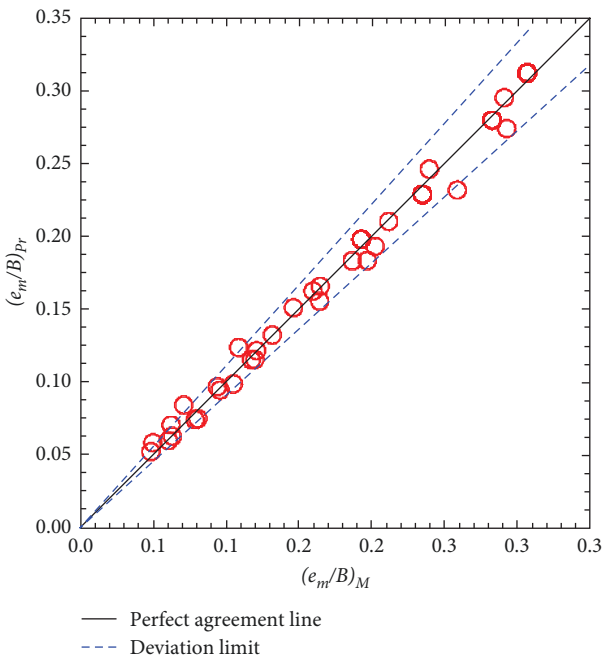

Figure 22: Comparison of $(e_m/B)_{pr}$ obtained from Equation (10) versus $(e_m/B)_M$.

Table 6: Comparison of Equations (8) and (10) in terms of number of independent variables and accuracy of predictions.

Equation	Number of independent variables	R^2	Adjusted R^2	RMSE
Equation (8)	5	0.992	0.992	0.0069
Equation (10)	3	0.992	0.992	0.0069

obtained by the program SUCH by about 11.4% and 6.1% for rafts of L/B ratios of 1.25 and 1.8, whereas for the raft of L/B ratio of 1.5, the predicted e_m values by Equations (8) and (10), and the program SUCH are equal, and Equation (4) at the values of the diffusion coefficients (i.e., $\alpha = 0.01$ and $0.05\ m^2/day$), the differences between the predicted e_m by Equation (8) or Equation (10) and the program SUCH are approximately $\pm 11\%$. Based on the above results, Equation (8) or Equation (10) can be used to estimate the value of e_m with the ability to be simply incorporated into an Excel sheet for practical use by practitioners and researchers.

5. Conclusions

This study offers a methodical approach for calculating the climate-controlled soil parameters, which are utilized to predict the 3D distorted mound shape beneath a flexible cover slab resting on expansive soils from the results of standard geotechnical tests. The suggested method was used to determine the climate-controlled parameters for expansive soils at various KSA locations, including equilibrium soil suction, the amplitude of surface suction change, diffusion coefficient, suction compression index, and active zone depth.

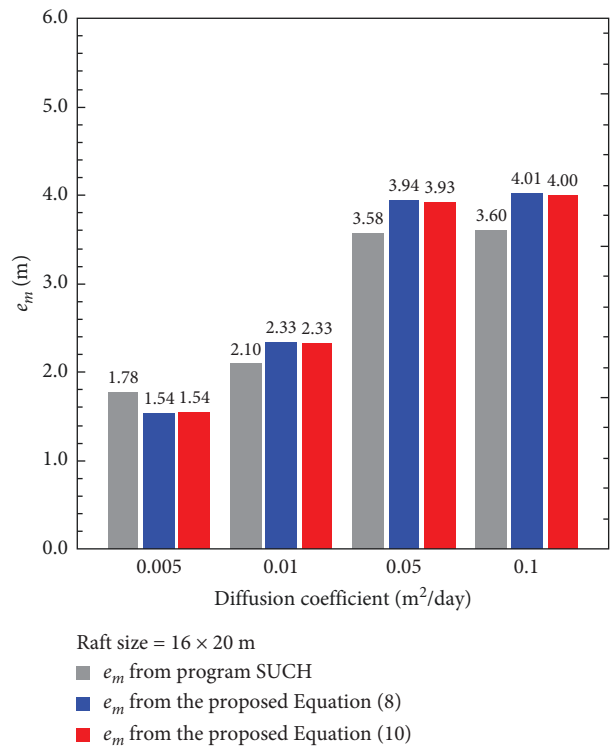

Figure 23: Comparisons among the e_m values obtained from the program SUCH, Equations (8) and (10) for raft of aspect ratio $L/B = 1.25$.

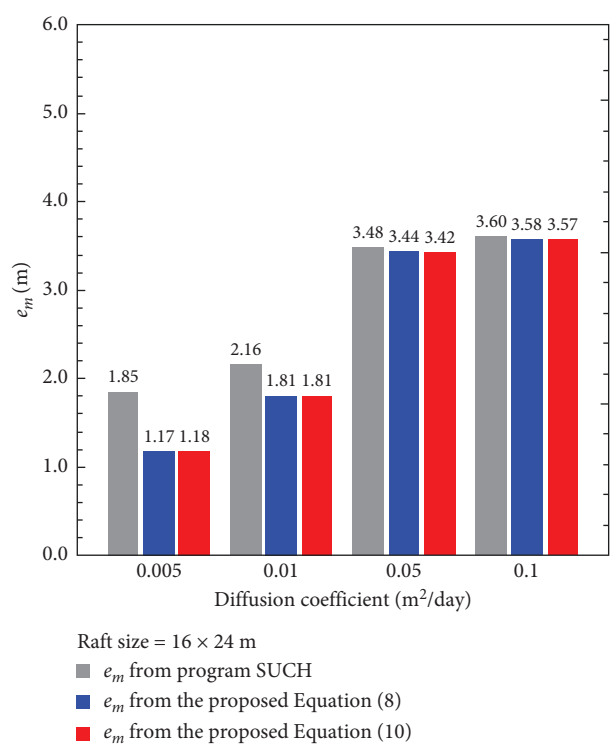

Figure 24: Comparisons among the e_m values obtained from the program SUCH, Equations (8) and (10) for raft of aspect ratio $L/B = 1.5$.

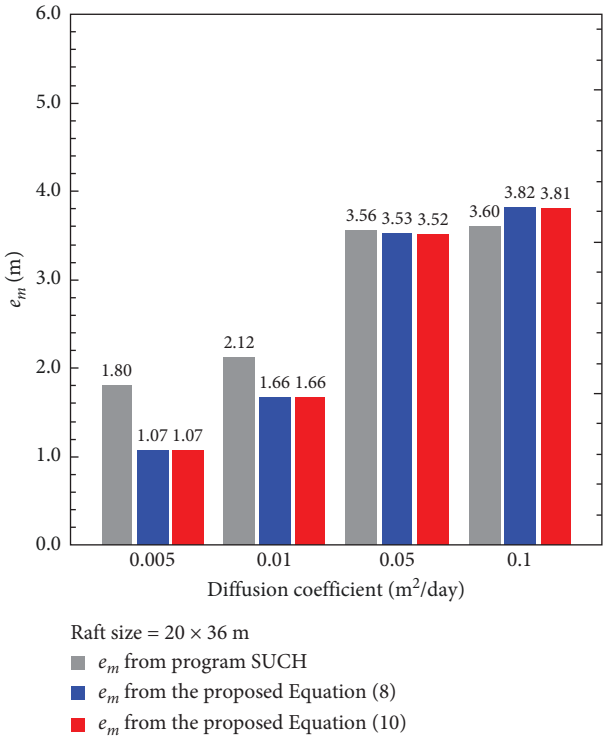

FIGURE 25: Comparisons among the e_m values obtained from the program SUCH, Equations (8) and (10) for raft of aspect ratio $L/B = 1.8$.

This method will greatly aid in the design of stiffened rafts using the current design methods. The SUCH program was used to study the effect of the climate-controlled soil parameters and raft dimensions on the shape of the deformed mound, its maximum differential movement, and its edge distance. Additionally, a formula is developed to calculate the edge moisture variation distance as a function of the raft's aspect ratio and climate-controlled soil parameters.

The following are the main conclusions drawn from the research's findings:

(1) The aspect ratio of the raft and the climate-controlled soil parameters have a significant impact on the shape of the distorted mound. The initial contact area between the distorted mound and the raft grows as the aspect ratio of the raft increases. For each raft, the initial contact area decreases with increasing diffusion coefficient and active zone depth, but there are no changes in this area with increasing suction compression index and the amplitude of surface suction change. In the consideration of the interaction between the stiffened rafts and the deformed mound of the expansive soil, the initial contact area is regarded as a key parameter.

(2) The maximal differential movement is unaffected by the raft dimensions and increases linearly with the amplitude of surface suction change and the suction compression index, as well as nonlinearly with the soil diffusion coefficient and the depth of the active zone.

(3) The edge distance is strongly influenced by the raft dimensions, the diffusion coefficient, and the depth of the active zone but is unaffected by the amplitude of surface suction change and the suction compression index.

(4) Although the proposed edge distance equation predicts values comparable to those calculated by the program SUCH, more validations are required for the equation against field measurements.

(5) The program SUCH overcomes the drawback in the current design methods of stiffened rafts that consider the distorted mound shape in 2D by simulating the distorted mound shape beneath a flexible cover slab in 3D using climate-controlled parameters of expansive soils and climatic conditions.

Data Availability

Data and models used to support the findings of this study are available from the corresponding author upon request.

Conflicts of Interest

The authors declare that they have no conflicts of interest.

Acknowledgments

This research is supported by the University of Tabuk (UT), Deanship of Scientific Research, under grant no. S-1443-0090. The author gratefully acknowledges this financial support.

References

[1] D. E. Jones Jr. and W. G. Holtz, "Expansive soils—the hidden disaster," *Civil Engineering*, vol. 43, no. 8, pp. 49–51, 1973.

[2] A. W. Dhowian, *Evaluation of Expansive Soils and Foundation Methodology in the Kingdom of Saudi Arabia*, General Directorate Research Grants Programs, King Abdulaziz City for Science and Technology, Riyadh, Kingdom of Saudi Arabia, Rep. AT-5-88, 1990.

[3] M. Dafalla and M. Al-Shamrani, "Geocharacteristics of tabuk expansive shale and its links to structural damage," in *Geo-Congress 2014 Technical Papers*, pp. 882–889, American Society of Civil Engineers, ASCE GSP No. 234, 2014.

[4] M. Dafalla, M. Al-Shamrani, and A. Al-Mahbashi, "Expansive soil foundation practice in a semiarid region," *Journal of Performance of Constructed Facilities*, vol. 31, no. 5, 2017.

[5] A. W. Dhowian, I. A. Ruwaih, and A. O. Erol, "The distribution and evaluation of the expansive soils in Saudi Arabia," *Proceedings of the Second Saudi Engineers Conference*, vol. 1, pp. 308–326, 1985.

[6] I. A. Ruwaih, "Experiences with expansive soils in Saudi Arabia," in *Proceedings of 6th International Conference on Expansive Soils*, pp. 317–322, Scientific Research Publishing, New Delhi, December 1987.

[7] S. N. Abduljauwad, "Swelling behaviour of calcareous clays from the eastern province of Saudi Arabia," *Quarterly Journal of Engineering Geology and Hydrogeology*, vol. 27, no. 4, pp. 333–351, 1994.

[8] J. Li, D. A. Cameron, and G. Ren, "Case study and back analysis of a residential building damaged by expansive soils," *Computers and Geotechnics*, vol. 56, no. 3, pp. 89–99, 2014.

[9] M. A. Dafalla, M. A. Al-Shamrani, A. J. Puppala, and H. E. Ali, "Use of rigid foundation system on expansive soils," in *GeoFlorida 2010*, pp. 1680–1689, American Society of Civil Engineers, ASCE GSP No. 199, 2010.

[10] J. D. Nelson, K. C. Chao, D. D. Overton, and E. J. Nelson, *Foundation Engineering for Expansive Soils*, John Wiley & Sons, Inc, 2015.

[11] M. A. Shams, M. A. Shahin, and M. A. Ismail, "Design of stiffened slab foundations on reactive soils using 3D numerical modeling," *International Journal of Geomechanics*, vol. 20, no. 7, 2020.

[12] S. F. Ahmad, "Foundations over expansive soil, a Saudi Arabia case history," in *5th Conference of the International Conference on Case Histories in Geotechnical Engineering*, pp. 1–8, University of Missouri–Rolla, New York, New York, April 2004.

[13] M. A. Dafalla and M. A. Shamrani, "Expansive soil properties in a semi-arid region," *Research Journal of Environmental and Earth Sciences*, vol. 4, no. 11, pp. 930–938, 2012.

[14] J.-L. Briaud, R. Abdelmalak, X. Zhang, and C. Magbo, "Stiffened slab-on-grade on shrink-swell soil: new design method," *Journal of Geotechnical and Geoenvironmental Engineering*, vol. 142, no. 7, Article ID 0001460, 2016.

[15] R. L. Lytton, *Design Criteria for Residential Slabs and Grillage Rafts on Reactive Clay*, Report for the Australian Commonwealth Scientific and Industrial Research Organization, Division of Applied Geomechanics, Melbourne, Australia, 1970.

[16] P. F. Walsh, "The design of residential slabs-on-ground," *CSRIO Australian Division Building Research Technology*, vol. 5, pp. 1–15, 1974.

[17] P. W. Mitchell, "The structural analysis of footings on expansive soil," in *Proc. 4th Intl. Conf. on Expansive Soils*, vol. 1, pp. 438–447, Denver, Colorado, 1980.

[18] J. E. Holland, W. G. Pitt, C. E. Lawrance, and D. J. Cimino, "The behavior and design of housing slabs on expansive soils," vol. 1, Denver, CO, pp. 448–468, 1980, Proc. 4th Intl. Conf. on Expansive Soils.

[19] PTI, *Design and Construction of Post-Tensioned Slabson-Ground*, Post Tensioning Institute, Phoenix, AZ, 3rd edition, 2004.

[20] B. M. El-Garhy, W. K. Wray, and A. A. Youssef, "Using soil diffusion to design raft foundation on expansive soils," *Advances in Unsaturated Geotechnics*, pp. 586–601, 2000.

[21] B. M. El-Garhy, A. A. Youssef, and W. K. Wray, "Predicted and measured suction and volume changes in expansive soil," Shizuoka, Japanpp. 55–64, 2001, Proc. of Intl Symposium on Suction, Swelling, Permeability and Structure of Clays.

[22] B. M. El-Garhy and W. K. Wray, "Method for calculating the edge moisture variation distance," *Journal of Geotechnical and Geoenvironmental Engineering*, vol. 130, no. 9, pp. 945–955, 2004.

[23] W. K. Wray, B. M. El-Garhy, and A. A. Youssef, "Three-dimensional model for moisture and volume changes prediction in expansive soils," *Journal of Geotechnical and Geoenvironmental Engineering*, vol. 131, no. 3, pp. 311–324, 2005.

[24] B. M. El-Garhy and W. K. Wray, "Investigation of a leaking water line beneath residential foundation on expansive soils," *Unsaturated Soils*, vol. 1, pp. 367–378, 2006.

[25] P. W. Mitchell, W. G. Kenneth, and Smith & Associates, *The Structural Analysis Of Footings On Expansive Soil*, Kenneth W. G. Smith & Associates, Adelaide, South Australia, 1980.

[26] W. K. Wray, "Using soil suction to estimate differential soil shrink or heave," Reston, Vapp. 66–87, 1997, Proc. Unsaturated Soil Engineering Practice ASCE GSP No. 68.

[27] A. M. Dhowian, *Evaluation of Expansive Soils and Foundation Methodology in the Kingdom of Saudi Arabia*, King Saud University Press, Riyadh, Saudi Arabia, 1989.

[28] A. O. Erol and A. Dhowian, "Swell behaviour of arid climate shales from Saudi Arabia," *Quarterly Journal of Engineering Geology and Hydrogeology*, vol. 23, pp. 243–254, 1990.

[29] T. M. Okasha and S. N. Abduljauwad, "Expansive soil in Al-Madinah, Saudi Arabia," *Applied Clay Science*, vol. 7, no. 4, pp. 271–289, 1992.

[30] T. Al-Refeai and D. Al-Ghamdy, "Geological and geotechnical aspects of Saudi Arabia," *Geotechnical and Geological Engineering*, vol. 12, no. 4, pp. 253–276, 1994.

[31] A. I. Al-Mhaidib, "Swelling behaviour of expansive shales from the middle region of Saudi Arabia," *Geotechnical and Geological Engineering*, vol. 16, no. 4, pp. 291–307, 1998.

[32] A. A. Sabtan, "Geotechnical properties of expansive clay shale in Tabuk, Saudi Arabia," *Journal of Asian Earth Sciences*, vol. 25, no. 5, pp. 747–757, 2005.

[33] S. A. Aiban, "Compressibility and swelling characteristics of Al-Khobar Palygorskite, eastern Saudi Arabia," *Engineering Geology*, vol. 87, no. 3-4, pp. 205–219, 2006.

[34] L. D. Johnson and W. R. Stroman, "Analysis of behavior of expansive soil foundations," Vicksburg, Technical Report S-76-8, Soils and Pavements Laboratory U. S. Army Engineer Waterways Experiment Station P. O. Box 631. Miss. 39180, 1976.

[35] R. Lytton, "Prediction of movement in expansive clays," vol. 2, pp. 1827–1845, 1994, ASCE GSP No. 40.

[36] G. D. Aitchison, "Statement of the review panel: Engineering concepts of moisture equilibria and moisture changes in soils beneath covered area," Butterworths, Australiapp. 7–21, 1965, Proc., Moisture Equilibria and Moisture Changes in Soils Beneath Covered Areas.

[37] AS 2870-2011, *Residential Slabs and Footings*, Australian Standards, NSW, Australia, 2011.

[38] J. D. Vann and S. L. Houston, "Field soil suction profiles for expansive soil," *Journal of Geotechnical and Geoenvironmental Engineering*, vol. 147, no. 9, Article ID 04021080, 2021.

[39] K. Russam and J. D. Coleman, "The effect of climatic factors on subgrade moisture conditions," *Geotechnique*, vol. 11, no. 1, pp. 22–28, 1961.

[40] D. A. Cameron, "Tests for reactivity and prediction of ground movement," *Australian Civil Engineering Transactions*, vol. CE31, no. 3, pp. 121–123, 1989.

[41] D. G. Fredlund and A. Xing, "Equations for the soil–water characteristics curve," *Canadian Geotechnical Journal*, vol. 31, no. 4, pp. 521–532, 1994.

[42] A. Johari, G. Habibagahi, and A. Ghahramani, "Prediction of soil–water characteristic curve using genetic programming," *Journal of Geotechnical and Geoenvironmental Engineering*, vol. 132, no. 5, pp. 661–665, 2006.

[43] A. Johari, G. Habibagahi, and A. Ghahramani, "Prediction of SWCC using artificial intelligent systems: a comparative study," *Scientia Iranica*, vol. 18, no. 5, pp. 1002–1008, 2011.

[44] R. G. McKeen, "Field studies of airport pavements on expansive clay," vol. 1, Denver, pp. 242–261, 1980, Proc. 4th Intl. Conf. on Expansive Soils.

[45] R. G. McKeen and L. D. Johnson, "Climate-controlled soil design parameters for mat foundations," *Journal of Geotechnical Engineering*, vol. 116, no. 7, pp. 1073–1094, 1990.
[46] R. McKeen, "A model for predicting expansive soil behavior," Dallaspp. 1–6, 1992, Proc., 7th Intl. Conf. on Expansive Soils.
[47] H. A. Perko, R. W. Thompson, and J. D. Nelson, "Suction compression index based on CLOD test results," *Advances in Unsaturated Geotechnics*, pp. 393–408, 2012.
[48] A. Johari and A. Hooshmand Nejad, "An approach to estimate wetting path of soil–water retention curve from drying path," *Iranian Journal of Science and Technology, Transactions of Civil Engineering*, vol. 42, no. 1, pp. 85–89, 2018.
[49] A. Johari and A. Talebi, "Stochastic analysis of rainfall-induced slope instability and steady-state seepage flow using random finite-element method," *International Journal of Geomechanics*, vol. 19, no. 8, Article ID 04019085, 2019.
[50] R. Jayatilaka and R. L. Lytton, "Prediction of expansive clay roughness in pavements with vertical moisture barriers," Texas A&M University, Transportation Institute, Texas, 1997, Report No. 0-187-28F, https://library.ctr.utexas.edu/hostedpdfs/tti/187-28F.pdf.
[51] R. Lytton, C. Aubeny, and R. Bulut, "Design procedure for pavements on expansive soils," vol. 1, , TxDOT, Austin, TX, TxDOT Designation FHWA/TX-05/0-4518-1, 2005.
[52] D. Mabirizi and R. Bulut, "Unified testing method for measuring diffusion coefficients for unsaturated soil drying and wetting in laboratory," *Transportation Research Record: Journal of the Transportation Research Board*, vol. 2170, no. 1, pp. 109–118, 2010.
[53] L. Chen and R. Bulut, "Numerical analysis of the effects of cracks on the moisture-diffusion coefficient of unsaturated soils," *International Journal of Geomechanics*, vol. 17, no. 8, 2017.
[54] A. B. Thakur, *Determination of diffusion coefficient through laboratory tests and analytically validating it using empirical relations for unsaturated soils*, MSc. Thesis, Texas A&M University, 2005.
[55] E. Yue and J. N. Veenstra, "Prediction of active zone depth in Oklahoma using soil matric suction," *Journal of GeoEngineering*, vol. 13, no. 1, pp. 29–38, 2018.
[56] R. L. Lytton, "Use of mechanics in expansive soil engineering," vol. 2, Dallas, Texas, pp. 13–25, 1992, Keynote Address, Proc. 7th Int. Conf. on Expansive Soils.